Published in final edited form as:
Conf Proc IEEE Eng Med Biol Soc. 2012 ; 2012: 3163–3166. doi:10.1109/EMBC.2012.6346636.

Performance enhancement and background removal to improve dynamic phase imaging of biological organisms

Katherine Creath [Member, EMBS, IEEE] and **Goldie Goldstein**
The authors are with 4D Technology Corporation, Tucson, AZ 85706 USA, and College of Optical Sciences, The University of Arizona, Tucson, AZ 85720 USA. K. Creath is also with Optineering, Tucson, AZ 85719 USA

Katherine Creath: kcreath@ieee.org; Goldie Goldstein: goldie.goldstein@4dtechnology.com

Abstract

This paper describes recent advances in enhancing optical imaging performance and removal of background shape for a new, novel interference dynamic microscope system. The specially designed optical system enables instantaneous 4-dimensional video measurements of dynamic motions within and among live cells without the need for labels or contrast agents. This instrument utilizes a pixelated phase mask enabling simultaneous measurement of multiple interference patterns. It incorporates the polarization properties of light to capture phase image movies in real time at video rates enabling tracking of dynamic motions and volumetric changes. Optical thickness data are obtained from phase images after processing to remove the background surface shape to quantify changes in cell position and volume. Data from a number of different biological organisms will be presented. These data highlight examples of the optical image quality and image processing.

I. Introduction

THE ability to instantaneously measure live cells, and follow motions and processes over time, provides valuable information to researchers studying cellular dynamics, motility, and cell and tissue morphology. Quantitative phase imaging can measure structures from interference images analogous to those viewed with phase-contrast, differential interference contrast and digital holography. Phase images reveal features and quantitative data not available through conventional imaging. Phase imaging quantifies optical thickness variations due to small variations in refractive index relating to variations in density of different structures and materials within cells and tissues. Very small refractive index variations can manifest large variations in optical thickness. Phase image data enable quantitative measurements that are not possible with standard microscopy techniques. [1–4] They can be directly combined and correlated with any other type of microscopic imaging such as fluorescence imaging. To obtain phase image data, harmless light levels are used, and samples do not need to be stained, labeled or marked. By taking short snapshots in rapid succession, the dimension of time opens up the ability to track motions of cells, see how cells interact with one another, and follow small motions within cells, tissues and structures. This type of imaging enables new studies involving cell tracking and process monitoring.

This paper presents an update on current research in developing a novel interference microscope specially designed for measurement of living and moving biological samples in liquids under cover slips. For these examples, objects are viewed in reflection; however, the method is easily adaptable to measurement in transmission, for use with immersion, or any other quantitative phase imaging technique. Here we discuss design techniques that have improved image quality and processing methods to remove background surface shape enabling better extraction of position and volumetric information.

II. Background

Techniques developed for full-field phase-imaging interference microscopes have historically relied upon temporal phase-measurement methods that obtain interferograms sequentially, and therefore require good vibrational damping with static specimens so that high-quality data can be obtained. [5] These techniques have been underutilized for biological measurements because they are sensitive to motion and vibration. [6–12] Interferometric microscopes generally employ narrowband illumination with short coherence lengths of tens of microns. The reason for narrowband “low coherence” illumination (short temporal coherence length) is to reduce effects of reflections off of nearby surfaces and to help reduce effects of speckle in the imaging systems. Further improvement in imaging quality can be obtained by incorporating extended low spatial coherence sources. With biological samples, this enables isolation in space without getting spurious interference patterns from other surfaces (mainly the cover slip). More details can be found in references. [1–4]

A. Dynamic Interference Microscope

The interference microscope used for this work is based upon a Linnik configuration. [5] It is comprised of a Köhler-type illumination system utilizing a low coherence extended source, and a simple imaging system as shown in Figure 1. An aperture stop enables controlling the size of the source in the entrance pupil of the microscope objectives, while a field stop enables easier alignment of the system.

The incoming illumination passes through a polarizing beam splitter before the microscope objectives creating orthogonally polarized test and reference beams. The relative irradiances of the object and reference beam can be balanced for maximum contrast by adjusting the angle of the polarizer. A quarter-wave plate (QWP) before the camera converts the two polarized beams to right- and left-handed circular polarization to produce interference fringes at the pixelated phase mask. For the measurements in this paper, samples in water or cell media are viewed in reflection through a cover slip. Sources with wavelengths of 660 nm and 785 nm were used with 20× NA 0.45, or 10× NA 0.3 objectives. The imaging “tube” lens magnification (combination of tube and FOV lenses) varies from 1× to 2.25×.

B. Extended Low Coherence Source

Standard practice in interference microscopy would be to use a temporally low coherence source like an LED. However, this reduces the temporal coherence length drastically and would require equal optical paths in both arms of the Linnik so that the temporal coherence

function overlaps with the spatial coherence function. [13, 14] Essentially this means that there would also need to be an equivalent amount of glass and liquid in the reference arm as in the test arm in order to get equal optical path lengths.

To get around this limitation, it has been shown that by tailoring the temporal and spatial coherence, dispersive media can be unmatched in both arms and still have the positive effects of low coherence. [13, 14] This is done by designing the source with a temporal coherence long enough to enable path length differences generated by the dispersive media (the cover slip and liquid), while reducing the spatial coherence to localize the interference fringes in space so that spurious reflections and coherent noise are not present.

To reduce the spatial coherence to 25–35 μm, a diode laser beam having a temporal coherence length of 250–300 μm was focused onto a rotating diffuser and coupled into an NA 0.22 multi-mode optical fiber with a 1 mm core. The laser has sufficient temporal coherence over path length differences that take into account the cover glass, while the spatial size of the source given by the exit face of the multimode optical fiber and the aperture stop will limit the spatial coherence.

C. Pixelated Phase Mask to Determine Phase

The polarization mask is comprised of an array of micropolarizers that are constructed from wire grid polarizers as shown in Figure 2. Wire-grid polarizers are made of tiny metal wires that are deposited on a transparent substrate (typically aluminum wires on a glass substrate). The line width, thickness and period of the wires are approximately 100nm, 120nm and 240nm respectively. These sub-wavelength structures have the property of reflecting light polarized parallel to the wires and transmitting light polarized perpendicular to them. They function as efficient polarizers over a wide range of wavelengths and angles.

Four simultaneous full-field interferograms are then synthesized by combining pixels of each phase type. [15, 16] One well-known means of determining phase is the simple four-frame algorithm,

$$\varphi(x, y) = \text{atan2}[C(x, y) - A(x, y) / D(x, y) - B(x, y)],$$

where atan2 is the modulo 2π arctangent function. This produces a modulo 2π (wrapped) phase map which then needs to be unwrapped using standard techniques. [17] This algorithm is applied to 2×2 cells relating to each camera pixel with a sliding window.

III. Improving Optical Performance

This system is designed to have different fields of view (FOV) using a flip-in FOV lens in the imaging arm. This effectively changes the total system magnification by a factor of up to 2.25×. With 20× objectives, this yields 20× and 45×. The Illunis XMV-2020 camera in this system has an active area of 9.2×8.88 mm yielding a 20× FOV of 460×440 μm and 204×197 μm at 45×.

Although the FOV lens increases the total system magnification by a factor of 2.25×, the optical resolution remains the same for a given objective. With 20× NA 0.45 objectives, the optical resolution is 0.9 μm (0.61 λ/NA). The sampling interval with the tube lens is 0.37 μm

and with the 2.25× FOV lens, it is 0.16 μm. The 20× total system magnification sampled the image close to Nyquist, and with 45× it is slightly over sampled. We are in the process of building a 50× NA 0.8 Linnik that will enable optical resolution of 0.5 μm with FOV's of 230 × 170 μm at 50× and 100 × 75 μm and samplings of 0.15 and 0.066 μm and will be presenting these measurements at the conference. The 50× will significantly improve measurement resolution.

To illustrate the relative fields of view, Figure 3 shows images of an Edmund Optics multi grid standard. The area has been cropped to provide a square FOV. Figure 4 shows a cross section of an image taken of a Ferritin Resolution Standard (Ted Pella, Cat. #608) having ferritin molecules with separations of 1.25 μm. Given the sampling of the image at 20×, there are approximately 4 pixels between ferritin molecules. The vertical lines indicate two adjacent ferritin molecules having a separation of ~1.2 μm. These molecules are clearly resolvable at 20×.

A. Effects of coherent and incoherent imaging

Earlier in this paper we discussed the importance of tailoring the spatial and temporal coherence. Figure 5 illustrates the effect of using a rotating diffuser to further improve illumination. Speckle from a 300 μm coherent length diode laser source can be seen in the left image. This coherence length ensures we are not seeing interference from nearby surfaces, but there is still obviously coherent noise present. The right images show improvement by introducing a rotating diffuser. The diffuser fills the entire NA 0.2, 1mm fiber diameter and therefore more modes of the multi-mode fiber. When the diffuser is rotated at a high speed, speckle will be averaged out to eliminate the coherent noise and generate a uniform extended source. This type of imaging is typically used in commercial interferometers for optical testing such as Fizeau and Twyman-Green interferometers, but has rarely been used in interference microscopes. This is because interference microscopes typically use temporally less coherent sources than those required to deal with biological object dispersion. In contrast, holographic microscopes need to use more coherent illumination in order to obtain sufficient fringe contrast. Clearly, our approach improves image quality and provides a spatially incoherent image. Figure 6 shows a single cross section profile through the phase measurements shown in the bottom of Figure 5. The noise in the phase is significantly reduced with the rotating diffuser.

B. Sample Phase Image

An in vitro cell culture of the MCF715 human breast cancer line was grown in cell media on cover slips at the University of Arizona Cancer Center. For these images, the cover slips were placed upside-down on a highly reflective mirror with cell media between the mirror and cover slip. These images were taken at 20× with a 1.67× FOV lens, a 660 nm source and 2 ms exposures. Figure 7 shows an image of some of these cells. Note that the intercellular matrix and newly forming cells around the edges of the matrix are clearly visible and easily resolved as are organelles and nuclei within the cells. The lateral sampling in the image for this exposure is 0.53 μm for each 4-pixel 2×2 cell in the pixelated phase mask. The optical resolution at NA=0.45 is 0.9 μm (0.61 λ/NA) yielding a slightly over sampled image.

IV. Processing to remove background shape

In order to obtain quantitative optical thickness data for the extraction of positional motion and/or volumetric changes, the objects of interest must be isolated from the background. Background removal is particularly difficult when there are a few large or numerous smaller objects that are changing within the field of view. One method that can be used for background shape suppression is to fit low-order Zernike polynomials [16] to the phase data across the entire array, generate a synthetic surface from the Zernike fit and subtract it from the original data. The difference between the data and the Zernike surface effectively isolates the objects and subtracts the low spatial frequency shape of the background surface.

This process serves two functions. Besides removing the background shape so that objects can be quantified relative to a flat surface, the mean value can be kept constant from frame to frame to aid in tracking quantitative changes with time. Figure illustrates this process on 3 frames of a sequence of images from a phase movie taken at 45× of a moving paramecium. Tilt and subtle shape are noticeable in the top images where the left side of the images is higher than the right side. This is removed in the bottom set of images enabling the isolation of the paramecium by itself. Another by product of this procedure is removal of the mean value from frame to frame. This effectively eliminates jumps between frames caused by noisy pixels, small pieces of debris in the cell solution or scratches on glass surfaces.

Another example with a ciliate taken at 15 Hz is shown in Figure. This protozoa is physically restricted in the liquid layer between the reflective mirror and the cover glass, and unable to swim. Cilia are clear in these images, but they are moving fast enough to blur a little with a 1 ms exposure. Movie files of Figures 8 and 9 are available online. [18]

V. Discussion and Conclusion

This paper has described recent research into development of a dynamic phase imaging microscope and has shown examples of 4D phase measurements of living biological organisms. Short exposure times freeze motion instantaneously. All the data to determine phase and optical thickness can be gathered in a single snapshot, so no scanning is necessary. Data from bright field imaging and phase contrast (interference image) are also obtained simultaneously along with phase and optical thickness. This model can also be extended to higher magnifications, immersion objectives, higher numerical apertures, a large range of wavelengths, and viewing cells in transmission as well as reflection. Harmless light levels offer a non-destructive means of observing and quantifying biological behavior and dynamic variations over time. The ability to dynamically measure biological organisms in real time opens up many different types of applications ranging from flow cytometry to tissue dynamics, morphological and volumetric studies along with mechanistic studies, process monitoring, quantification of cellular motion, monitoring and tracking cellular damage under known perturbations, tracking cell migration, nerve and muscle transmission, histology and photodynamic therapy. Conceptually, this model could be further modified to include simultaneous fluorescence measurements to more specifically track particular mechanisms.

Acknowledgments

We thank our 4D Technology colleagues Tim Horner, Mark McKune, Richard Robinson, Neal Brock, and James Millerd for their contributions to this project, as well as Andrew Rouse from The University of Arizona for cancer cell cultures.

This work was supported in part by NIH/NCRR 1R43RR028170-01, 2R44RR028170-02, and NIH/NIGMS 8R44GM103406-03.

References

1. Creath K. Dynamic quant. phase images of pond life, insect wings, and in vitro cell cultures. Proc. SPIE. 2010; 7782:77820B.
2. Creath K. Dynamic phase imaging utilizing a 4-dimensional microscope system. Proc. SPIE. 2011; 7904:79040O.
3. Creath, K. Dynamic Phase Imaging for in Vitro Process Monitoring and Cell Tracking. Proceedings of the 33rd Annual International Conference of the IEEE EMBS; Boston, Ma. August 29-September 3, 2011; 2011. p. 5977-5980.
4. Creath K, Goldstein G. Dynamic phase imaging and processing of moving bio. organisms. Proc. SPIE. 2012; 8227:82270M.
5. Schmit, J.; Creath, K.; Wyant, JC. Ch. 15. Surface Profilers, Multiple Wavelength, and White Light Interferometry. In: Malacara, D., editor. Optical shop testing; 3rd Edition. 3rd ed ed. Hoboken, NJ: Wiley-Interscience; 2007. p. 667-755.
6. Dunn GA, Zicha D. Phase-Shifting Interference Microscopy Applied to the Analysis of Cell Behaviour. Symposia of the Society for Experimental Biology. 1993; 47:91–106. [PubMed: 8165581]
7. Tychinsky VP, et al. Quantitative real-time analysis of nucleolar stress by coherent phase microscopy. Journal of Biomedical Optics. 2008; 13:064032. [PubMed: 19123678]
8. Yang C, et al. Phase-referenced interferometer with sub wavelength and sub hertz sensitivity applied to the study of cell membrane dynamics. Optics Letters. 2001 Aug.26:1271–1273. [PubMed: 18049583]
9. Popescu, G. Quantitative Phase Imaging of Nanoscale Cell Structure and Dynamics. In: Jena, BP., editor. Methods in Nano Cell Biology, Volume 90. Vol. 90. San Diego: Elsevier; 2008. p. 87-115.
10. Reed J, et al. High throughput cell nanomechanics with mechanical imaging interferometry. Nanotechnology. 2008 Jun.19
11. Yu LF, et al. Quantitative phase evaluation of dynamic changes on cell membrane during laser microsurgery. Journal of Biomedical Optics. 2008 Sep-Oct;13
12. Popescu, G. Quantitative Phase Imaging of Cells and Tussues. New York: Mc-Graw Hill; 2011.
13. Abdulhalim I. Competence between spatial and temporal coherence in full field optical coherence tomography and intererence microscopy. J Opt A: Pure Appl. Opt. 2006; 8:952–958.
14. Ryabukho V, Lyakin D. Longitudinal pure spatial coherence of a light field with wide frequency and angular spectra. Optics Letters. 2005; 30:224–226. [PubMed: 15751866]
15. Creath, K. Phase-measurement interferometry techniques. In: Wolf, E., editor. Progress in Optics. Vol. 26. Amsterdam: Elsevier Science Publishers; 1988. p. 349-393.
16. Malacara, D. Optical shop testing. 3rd ed ed.. Hoboken, NJ: Wiley-Interscience; 2007.
17. Ghiglia, DC.; Pritt, MD. Two-Dimensional Phase Unwrapping: Theory, Algorithms and Software. New York: Wiley; 1998.
18. http://www.u.arizona.edu/~kcreath/mov/embc/2012movies.html.

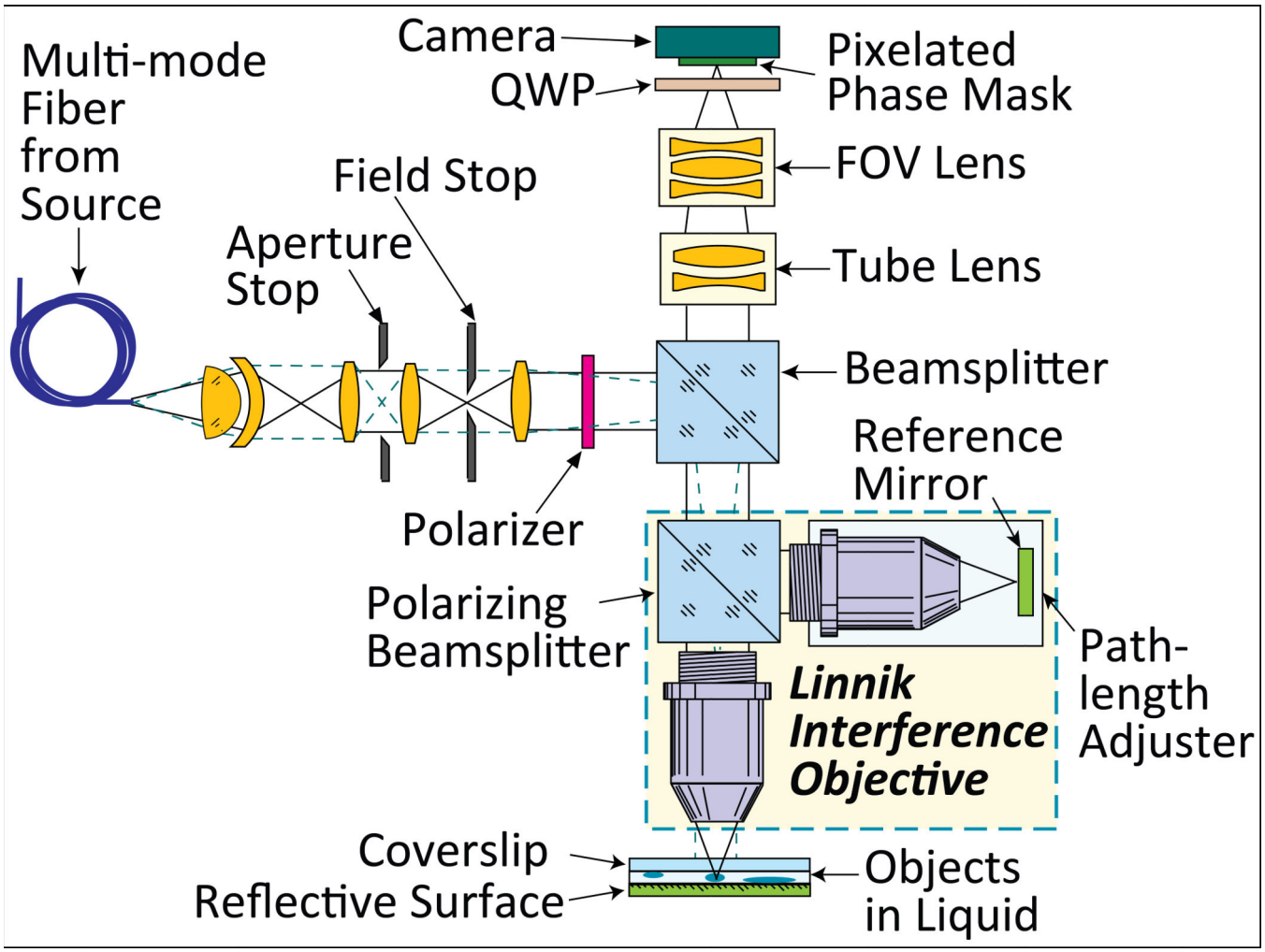

Figure 1.
Optical schematic of dynamic interference microscope.

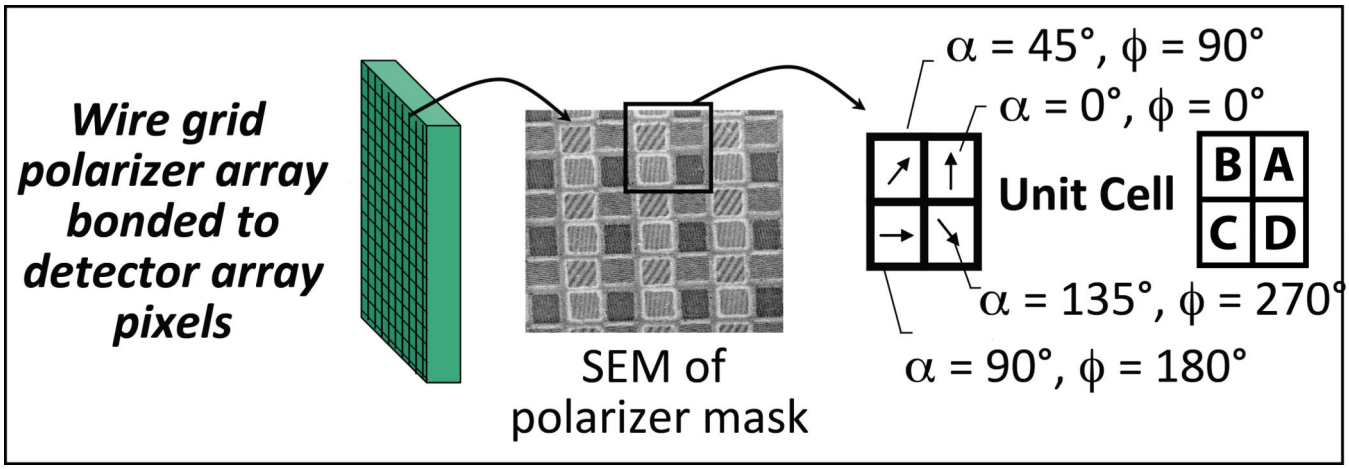

Figure 2.
Pixelated phase mask sensor is an array of wire grid micropolarizers on a glass substrate bonded to the detector array.

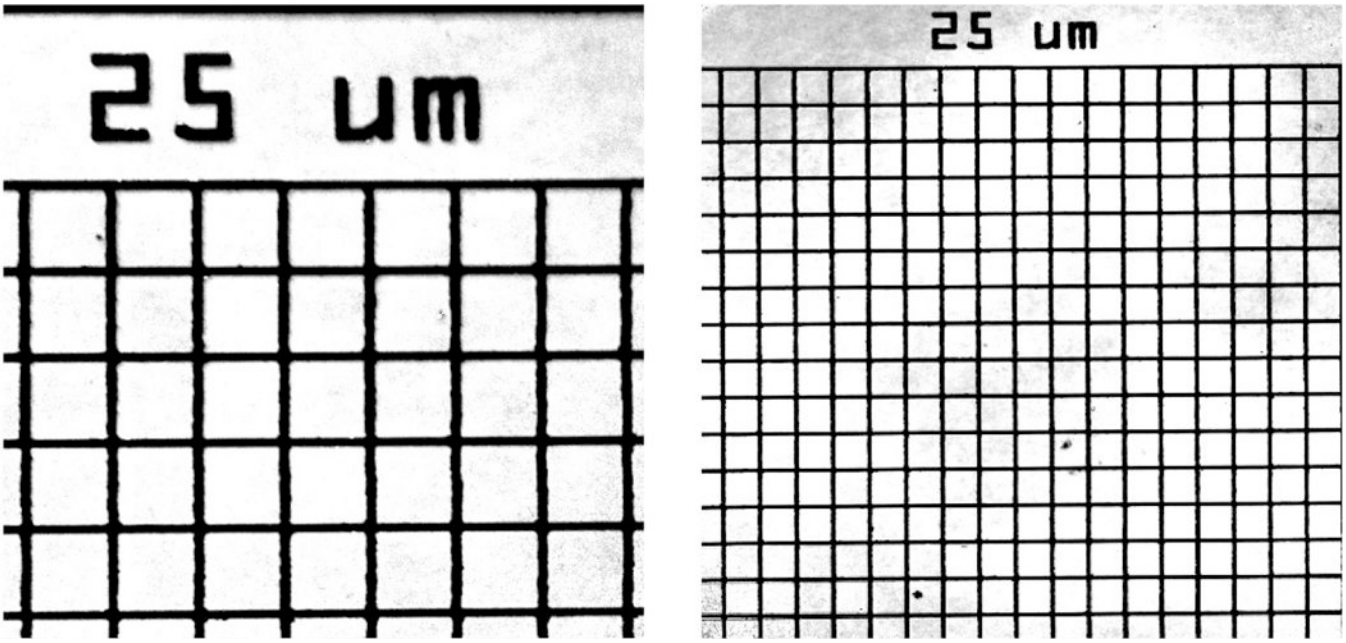

Figure 3.
Images of Edmund Optics multi grid standard at 20× and 45×.

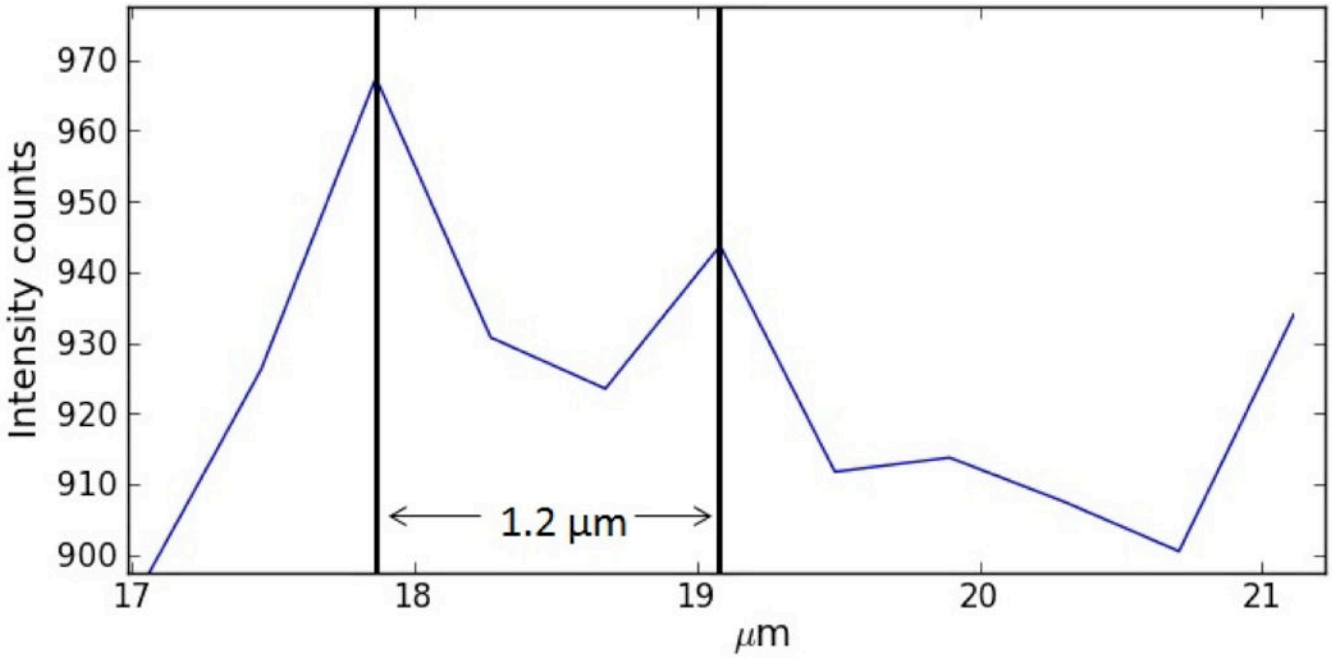

Figure 4.
Cross-section profile of ferritin molecules having a separation of 1.25 µm at 20×.

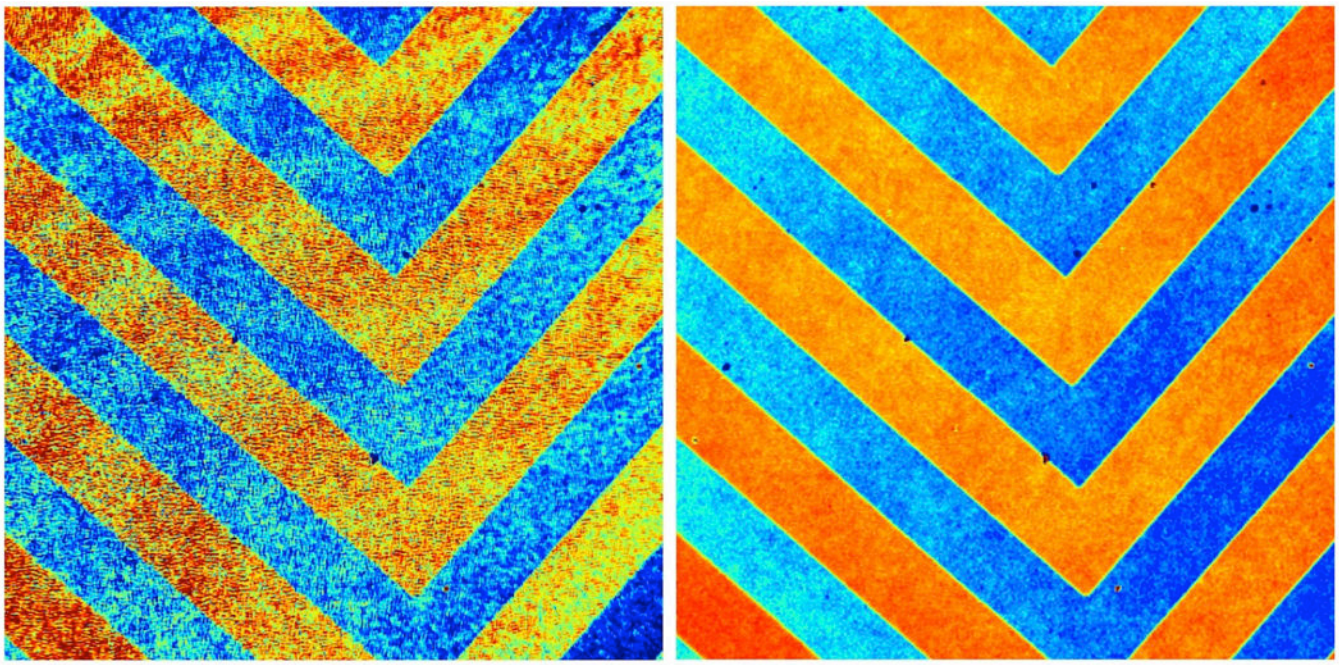

Figure 5.
Phase images of VLSI step height standard taken with (left) diode laser, and (right) with addition of rotating diffuser.

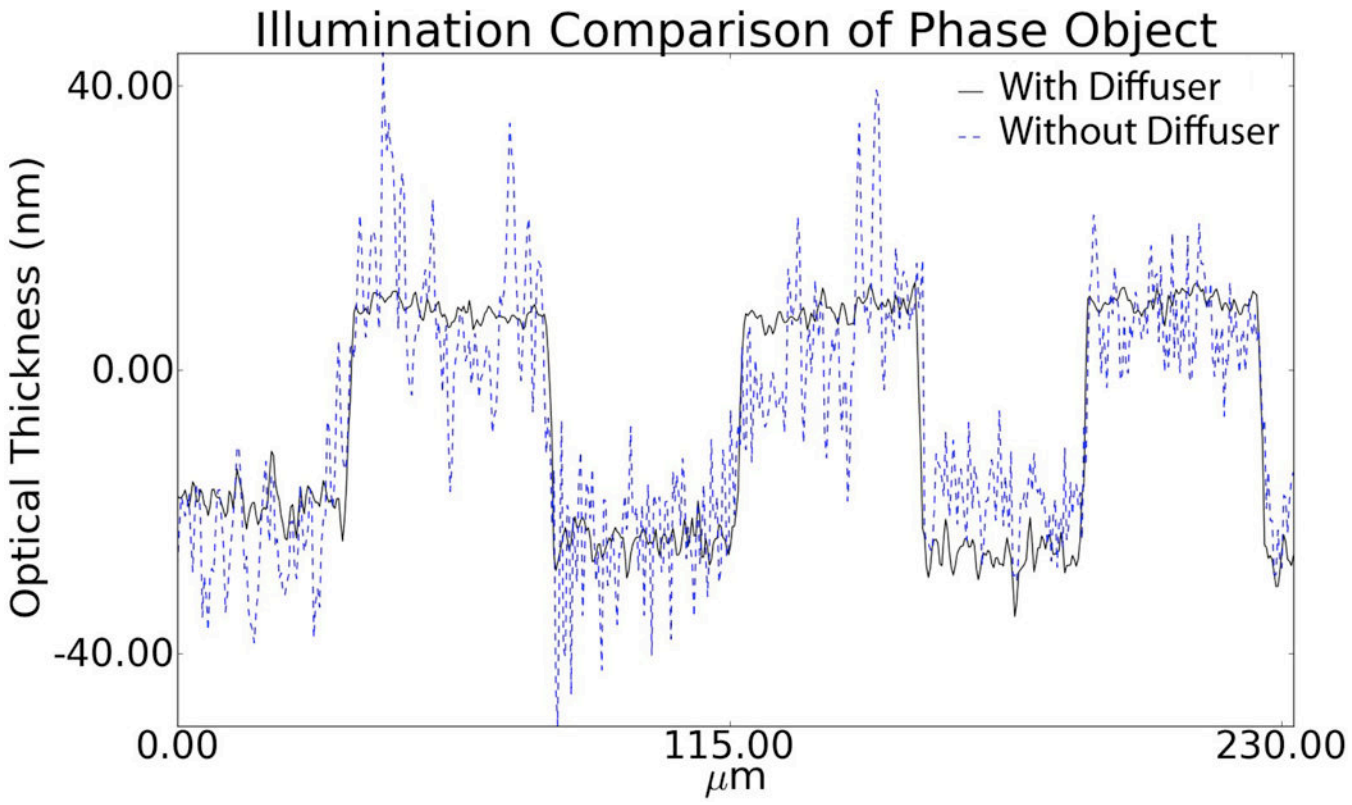

Figure 6.

Solid black line shows a cross section through a phase measurement using the rotating diffuser, whereas the dotted blue line is a measurement using a diode laser source without the diffuser.

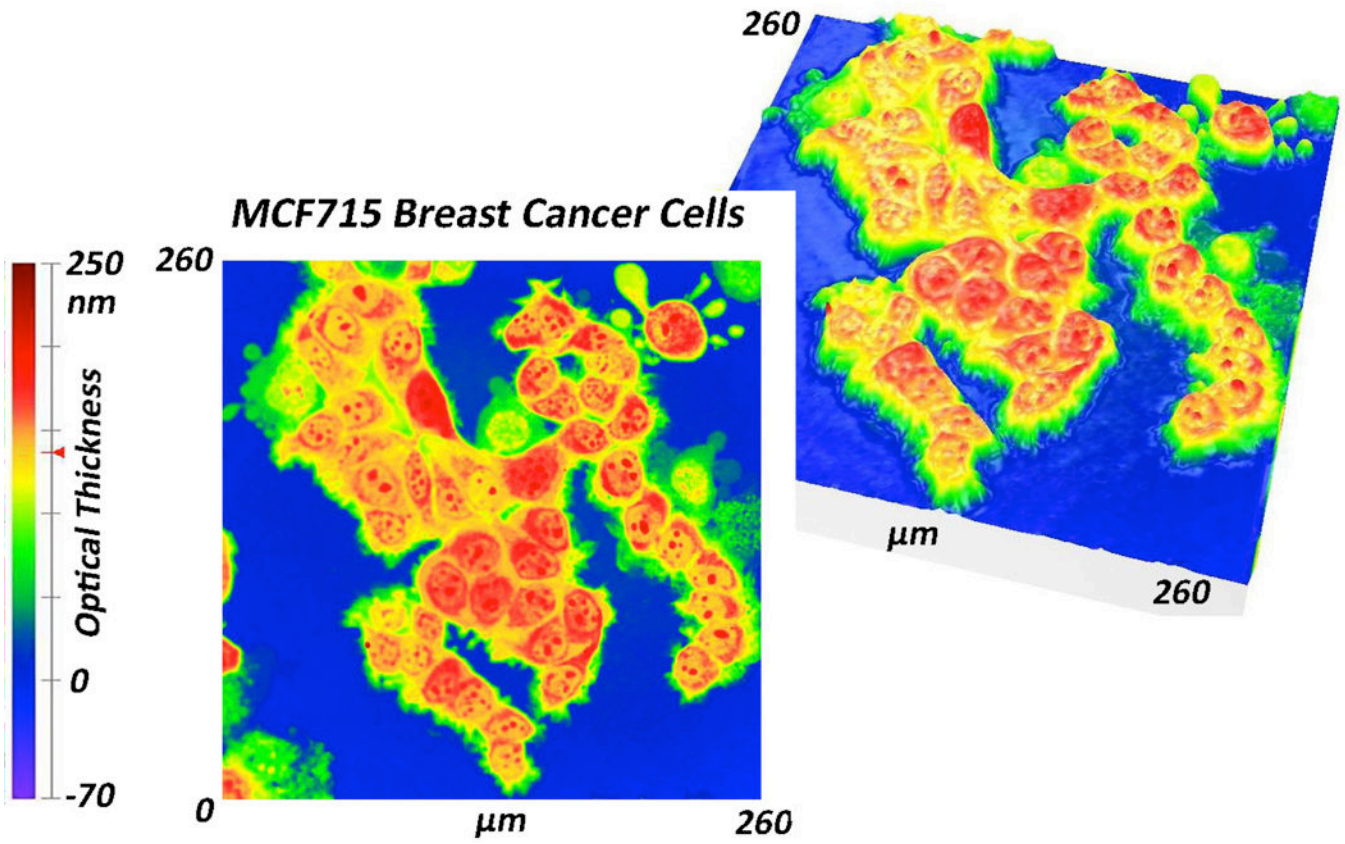

Figure 7.

Phase images showing contour and 3D view of human breast cancer cells. Notice cells and matrix forming that look fuzzy without organelles.

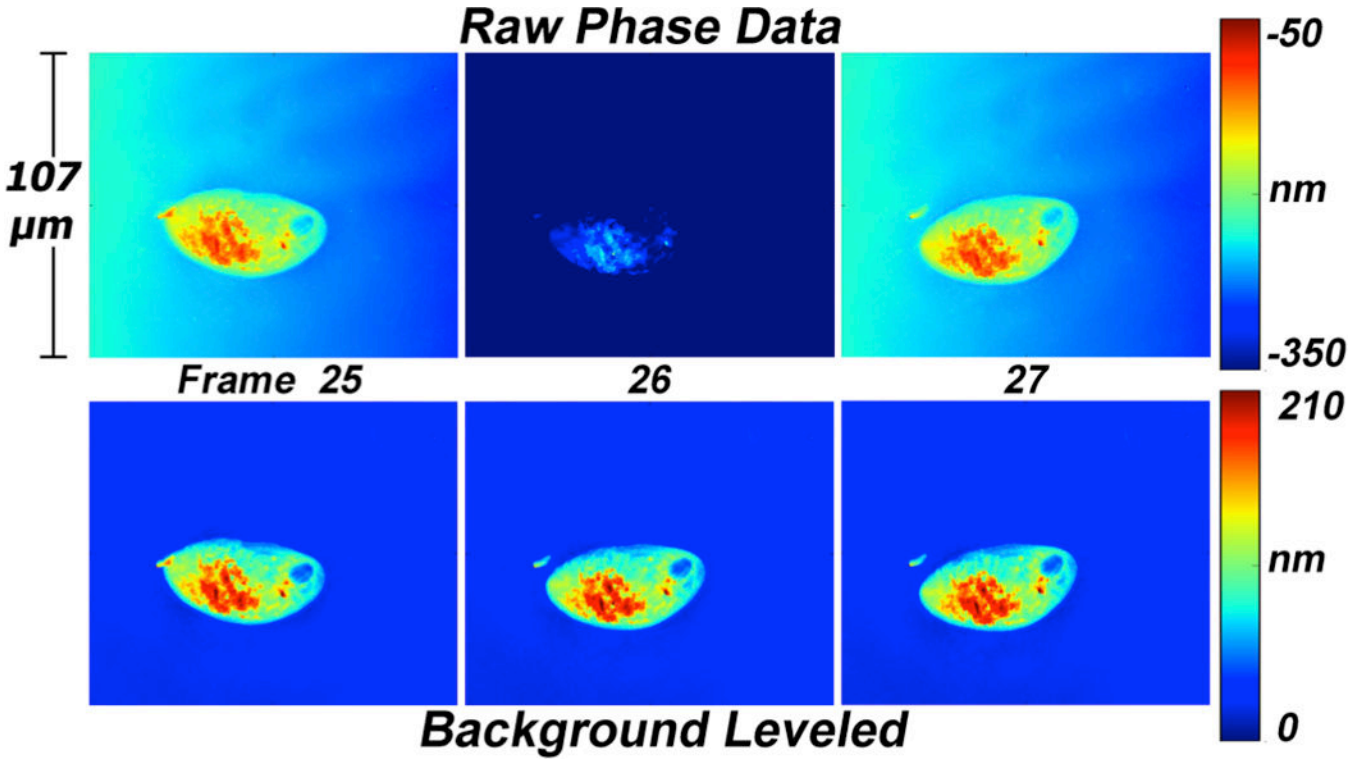

Figure 8.
(top) Raw phase data. (bottom) After background subtraction.

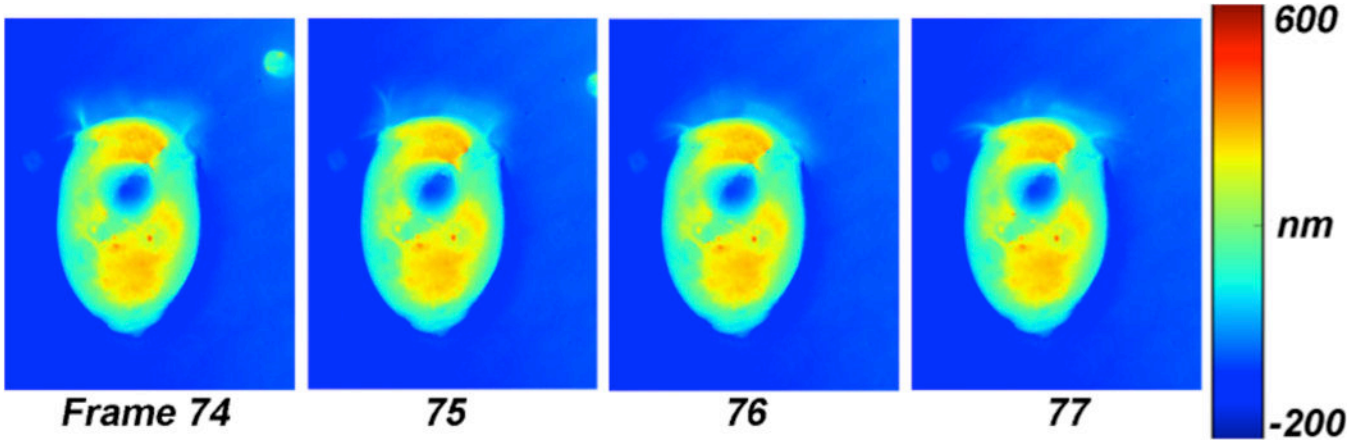

Figure 9.
Frames from movie of a ciliate taken at 46× with a 660 nm source. FOV is 84 × 104 μm.